Journal of Power Sources 188 (2009) 592–600

Contents lists available at ScienceDirect

Journal of Power Sources

journal homepage: www.elsevier.com/locate/jpowsour

Quantifying tortuosity in porous Li-ion battery materials

Indrajeet V. Thorat[a], David E. Stephenson[a], Nathan A. Zacharias[a], Karim Zaghib[b], John N. Harb[a], Dean R. Wheeler[a,*]

[a] Department of Chemical Engineering, Brigham Young University, Provo, UT 84602, United States
[b] Institut de Recherche d'Hydro-Qubec, 1800 Lionel Boulet, Varennes, QC, Canada J3X1S1

ARTICLE INFO

Article history:
Received 5 November 2008
Received in revised form 9 December 2008
Accepted 10 December 2008
Available online 24 December 2008

Keywords:
Tortuosity
Li-ion battery
Porous electrodes
Ionic mass transport
$LiFePO_4$

ABSTRACT

An accurate assessment of liquid-phase mass transport resistances is necessary for understanding and optimizing battery performance using mathematical models. This work combines modeling and experiments to quantify tortuosity in electrolyte-filled porous battery structures (separator and active-material film). Tortuosities of separators were measured by two methods, AC impedance and polarization-interrupt, which produced consistent results. We measured an apparent interfacial resistance at the lithium metal electrodes that contributed to both ohmic and diffusional resistance of the cell. The polarization-interrupt experiment was used similarly to measure effective electrolyte transport in porous films of cathode materials, particularly films containing $LiFePO_4$. An empirical relationship between porosity and the tortuosity of the porous structures was developed. Our results demonstrate that the tortuosity-dependent mass transport resistance in porous separators and electrodes is significantly higher than that predicted by the oft-used Bruggeman relationship.

1. Introduction

Lithium-ion batteries are widely used in consumer electronic devices. New applications like hybrid electric vehicles (HEVs) and plug-in-hybrid electric vehicles (PHEVs) are potential candidates for using Li-ion batteries. To achieve required energy and power densities, it is necessary to optimize batteries by understanding, quantifying, and mitigating the dominant resistances. One approach to increased understanding has been the use of macro-homogeneous mathematical models [1–9]. The effectiveness of such models depends to a large extent on the accuracy of the physical parameters used. The purpose of this work is to examine and increase the accuracy of the parameters that describe liquid-phase mass transport in electrodes and separators used in Li-ion batteries.

Porous electrodes and separators are multi-phase structures that include a network of interconnected and irregular pores or channels. It is difficult and time consuming to model these complicated pore networks in full three-dimensional realism. Instead, for macro-homogeneous models, the complexity of mass transport in the pore network is reduced to only one effective geometric parameter, tortuosity τ. The tortuosity of a porous network is used to obtain effective transport properties. It is assumed that the tortuosity affects transport properties, liquid-phase diffusivity and conductivity, with a similar functionality [10]. In general,

$$\kappa_{\text{eff}} = \frac{\kappa\epsilon}{\tau} \tag{1}$$

or

$$D_{\text{eff}} = \frac{D\epsilon}{\tau}. \tag{2}$$

Here κ_{eff} and κ are the effective and intrinsic conductivities, respectively, and D_{eff} and D are the effective and intrinsic diffusivities, respectively, of the conductive phase (in the present case the liquid electrolyte). Eqs. (1) and (2) serve as the definition of τ used in the present work. When comparing τ values from different sources, one must be cognizant of the definitions used. For example, our tortuosity is the square of the one used by Abraham [11]. Alternatively, some workers choose to describe effective conductivity in terms of a MacMullin number [12], which in this context is $N_{\text{M}} = \tau/\epsilon$.

The effective transport properties are corrected by ϵ, the volume fraction of the conductive phase (in the present case ϵ is the porosity or void fraction of the solid). This means that any salt molar fluxes (from D_{eff}) or electrical current densities (from κ_{eff}) in the model are based on superficial electrode and separator areas. If the conductive pathways are composed of straight channels of uniform cross section that are parallel to the transport direction, then $\tau = 1$ in Eqs. (1) and (2). Otherwise, for tortuous pathways $\tau > 1$ and effective transport properties are always lower than the intrinsic transport properties of the conductive phase.

Of course, τ depends in a complicated way on the structure of the porous network, including the nature and particle-size distribution

* Corresponding author. Tel.: +1 801 422 4126; fax: +1 801 422 0151.
E-mail address: dean_wheeler@byu.edu (D.R. Wheeler).

0378-7753/$ – see front matter © 2008 Elsevier B.V. All rights reserved.
doi:10.1016/j.jpowsour.2008.12.032

of each of the materials used in the porous electrode. Due to these complexities, researchers have used τ as an adjustable parameter or perhaps as a function of ϵ [10,13]. The Bruggeman relationship [11,14–17] has often been used to correlate and predict effective conductivities:

$$\kappa_{\text{eff}} = \kappa\epsilon^{\alpha}, \tag{3}$$

or equivalently,

$$\tau = \epsilon^{1-\alpha}, \tag{4}$$

where α is the Bruggeman exponent. For a system composed of a continuous conductive phase (e.g. liquid electrolyte) mixed with insulating spherical particles of uniform size (i.e. monodisperse) it has been shown empirically [16,17] that $\alpha \approx 1.5$. This value of α is often used in battery simulations.

There is almost a complete lack of direct experimental data for tortuosity or liquid-phase transport resistance in porous electrodes. Similarly, few have questioned the accuracy of the Bruggeman equation (Eq. (3)) with $\alpha = 1.5$. A few researchers [10–12] have used larger values of the Bruggeman exponent. Patel et al. [12] performed numerical simulations of porous networks with different morphologies and calculated the tortuosity for these networks in terms of a Bruggeman exponent. They also performed liquid-phase conductivity measurements for different types of battery separators and calculated corresponding Bruggeman exponents.

Prior work by our group [18] found that liquid-phase transport resistance in $LiCoO_2$ cathodes has a great effect on cell performance and that the usual Bruggeman relation with $\alpha = 1.5$ significantly underpredicts mass-transport resistances. While one can regress needed physical parameters by comparing cell performance to a full-cell-sandwich model (as we did), the presence of multiple unknown resistances (including kinetic and electronic transport) in the model makes accurate determination of one particular resistance difficult. Therefore, it is of great interest to develop an experimental approach to quantify directly the tortuosity or the liquid-phase transport resistance for porous electrode films and separators. We are not aware of prior experimental evaluation of the tortuosity of porous electrodes independent of other processes in the cell.

In this work we present techniques to determine the tortuosities of different Li-ion active-material films ($LiFePO_4$ and $LiCoO_2$) and one type of battery separator (Celgard 2400). Experiments included AC impedance to obtain κ_{eff} and a polarization-interrupt method to obtain D_{eff}, each performed on cells with a symmetric geometry and using an electrolyte with known intrinsic transport properties κ and D. The computer model described below was developed for interpreting the experiments and is essential for the success of the method. The use of two complementary experiments, one for κ_{eff} and one for D_{eff}, and of different thicknesses of materials serve to validate the results. Finally, we present a summary plot of the results showing the effect of porosity on the tortuosity of the active-material films.

2. Correlating tortuosity

As indicated by the above correlations (Eqs. (1) and (2)) the porosity ϵ plays an important role in the electrochemical performance of an electrode. Lower porosity corresponds to a greater fraction of solid particles including carbon, and hence a greater number of possible electronic pathways. This means that lower porosity is desired for lower electronic resistance [19]. On the other hand, higher porosity or liquid volume fraction is desired for lower liquid-phase transport resistance. Therefore, to optimize battery for a particular application, it is important to know the effect of porosity on the liquid-phase resistance in the electrode.

In this work, we use a generalized form of the Bruggeman relation [14] to correlate tortuosity:

$$\tau = \gamma\epsilon^{1-\alpha}, \tag{5}$$

where γ and α are the constants that could depend on the morphology, porosity, material, and particle-size distribution of a porous composite. Table 1 summarizes some prior published experimental work in terms of Eq. (5). As shown, most of the prior work involves either setting $\gamma = 1$ and adjusting α, or setting $\alpha = 1.5$ and adjusting γ, in order to obtain the needed τ value. Without multiple experiments at different ϵ values, one cannot determine the proper relationship between τ and ϵ, if any.

Patel et al. [12], Djian et al. [20], and Abraham [11] calculated tortuosities for different types of separators. For Celgard 2400 separators, these groups reported different values for the tortuosities. However, the Celgard 2400 samples used by these groups appear to have different porosities. The separator used in this work has the same porosity as that used by Patel et al.

Table 1 also compares tortuosities calculated for porous electrodes and for a packed bed. The Bruggeman approximation was reconfirmed by Patel et al. [12] and Pavlin et al. [21] for conductivity in a continuous phase mixed with uniform-size spherical particles. However, from numerical simulations for different particle shapes, Patel et al. [12] found that the tortuosity was higher than that predicted by the Bruggeman relation. Also, Doyle et al. [10] for $LiMn_2O_4$ electrodes and Stephenson et al. [18] for $LiCoO_2$ electrodes found that the tortuosity for the porous electrodes is significantly higher than the traditional Bruggeman relationship. However, these two works used discharge curves to fit τ as an adjustable parameter. The cell examined by Doyle et al. contained a gelled electrolyte, consequently the reported tortuosity accounts not only for the pores between active-material particles, but also for the transport retardation effect from intimate mixing of polymer and liquid electrolyte. As researchers have used tortuosity of cathode-material films as an adjustable parameter in their full battery simulations, the reported tortuosity values may inadvertently incorporate the effects of other processes (kinetics, transport, and thermodynamics) not accurately captured by the model. To accurately quantify the liquid-phase transport resistance or tortuosity, it is imperative to isolate the liquid-phase transport processes from the other processes in the electrode. This work presents experimental and modeling techniques that are developed to separate as much as possible the liquid-phase transport resistances from other processes.

Table 1
Reported tortuosities in the form $\tau = \gamma\epsilon^{1-\alpha}$ for selected porous structures.

Author	γ	α	τ	ϵ	Porous structure
MacMullin and Muccini [17]	1	1.6–1.7	4–5	0.1	Bed of spherical sandstone particles
Abraham [11]	7.3	1	7.3	0.32	Separator (Celgard 2400)
Djian et al. [20]	1	2.46	5.3	0.32	Separator (Celgard 2400)
Patel et al. [12]	1	2.8	6.0	0.37	Separator (Celgard 2400)
Doyle et al. [10]	1	3.3	2.9	0.63	$LiMn_2O_4$ electrode
Stephenson et al. [18]	18	1.5	21–27	0.43–0.71	$LiCoO_2$ electrode

3. Experimental procedure

This section describes the experimental techniques used to fabricate cells and quantify liquid-phase transport processes for a separator (Celgard 2400) and for free-standing porous cathode films.

3.1. Cell fabrication

To quantify the tortuosity of the porous structures, a symmetric cell geometry was used that is consistent with the method of restricted diffusion. Restricted-diffusion experiments involve one-dimensional diffusion in cells closed at the ends and in which concentration variations take place over the entire length between the ends [22,23]. Fig. 1 is a schematic of the cell geometry used to determine the tortuosity of the separator. The cells were assembled in an Ar-atmosphere glove box (moisture content 0.9 ppm and oxygen content < 0.25 ppm, VAC, Hawthorne, CA). Lithium metal foil (Alfa Aesar) of area 4 cm^2 on a copper current collector was used for each electrode. The two lithium electrodes were separated by 25-μm-thick polypropylene separator layers (Celgard 2400, Celgard LLC, Charlotte, NC). Metalized polymer film (Class PPD Shield Pack, Inc., Los Angeles, CA) was used to enclose the cells. Electrolyte composed of 1 M $LiPF_6$ in a 1:1 (w:w) mixture of ethylene carbonate and diethyl carbonate (LithDyne Elyte, LithChem International, Anaheim, CA) was added to the pouch before sealing with an electric heat sealer (Impulse Sealer Tish 200, Electronic Heating Equipment Co.). The cells were tested under external compression of 68 kPa above atmospheric pressure.

A geometry similar to Fig. 1 was used to quantify the transport properties for active-material films as shown in Fig. 2—the main difference is the presence of a free-standing active-material film placed between the two lithium electrodes. Separator layers electronically isolated the active-material film from the lithium electrodes as shown in Fig. 2. The active-material films were fabricated with one of two different active materials ($LiFePO_4$ or $LiCoO_2$) and delaminated from their current collectors as described below. In this paper by convention we refer to the free-standing active-material films or cathode films based on their composition and structure, not their function; the true electrodes in our experimental cells were always a pair of lithium foils.

Each active-material film contained (on a dry basis) 84 wt% active material, either $LiFePO_4$ (Hydro Qubec, Montral, Canada)

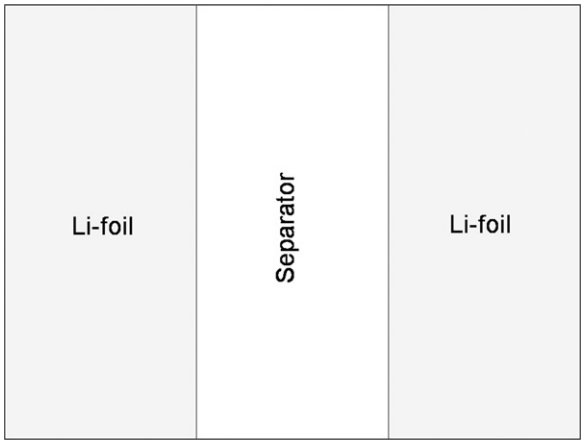

Fig. 1. Schematic of a symmetric cell geometry for testing separators. Lithium foils are used as anode and cathode, between which are placed one or more separator layers filled with the electrolyte.

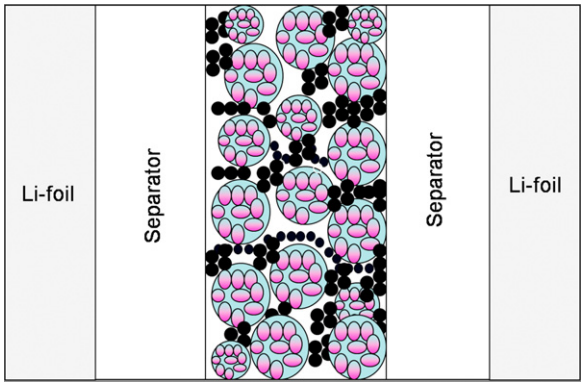

Fig. 2. Schematic of a symmetric cell geometry for testing porous-electrode films. The active-material film is delaminated from its current collector and placed between separators, which in turn are placed between lithium foil electrodes.

or $LiCoO_2$ (Alfa Aesar), along with 4 wt% carbon black (diameter: 20–30 nm, XC-72R, Cabot Carbon Ltd.), 4 wt% graphite (diameter: 5.5–7.5 μm, SFG-6, TIMCAL Group), and 8 wt% polyvinylidene fluoride copolymer (PVdF, 741 Kynar Corp.). In the case of carbon-fiber-containing $LiFePO_4$-material films, the graphite and carbon black components (8 wt% total) were replaced by carbon fibers (diameter: 100–200 nm, length: 30–100 μm, PR-19, Pyrograf Products Inc.). To fabricate the active-material film, PVdF was dissolved in NMP solvent (1-methyl-2pyrrolidone fluoride) with mild heating. The active-material and carbon components were dry-mixed with a spatula followed by mixing with an ultrasonic homogenizer. This solid mixture was then mixed with the solution of PVdF and NMP with a spatula followed by mixing with the ultrasonic homogenizer to form a composite slurry. Then, this composite slurry was spread onto an aluminum current collector with a doctor blade (Byk-Gardner, USA) to a desired wet thickness. To facilitate later delamination the slurry was applied to the shiny (thicker oxide) side of the aluminum foil without the benefit of an adhesion layer. The composite cast was dried overnight at 120° C under vacuum (15 mmHg).

Individual active-material films were cut from the dried composite cast using a template of 10 cm^2 area. The area of the active material films was larger than that of the lithium electrodes to make sure that transport of all lithium ions between electrodes took place only through the active material film. The active-material films were compressed to different thicknesses using a calendering machine (Pepetools, OK). From weight and thickness measurements, we calculated the porosities of the active-material films. After the calendering, the aluminum current collector was carefully removed from these active-material films using a 0.009-inch single-edge razor blade as shown in Fig. 3, with care taken to minimize bending of the films. The delaminated active-material film was then assembled into a pouch cell as previously discussed. Once the cell was fabricated, it was tested using the procedures described below.

3.2. Cell testing

The tortuosity of the separator or active-material films was obtained from two methods: polarization-interrupt (or restricted diffusion) and AC-impedance. The polarization-interrupt test was performed on assembled cells to obtain the effective diffusivity of the electrolyte. Similarly, AC impedance was performed on the assembled cells to calculate the effective conductivity of the electrolyte. In each case the effective diffusivity or conductivity was used to calculate the tortuosity of the porous structure using Eqs. (1) or (2).

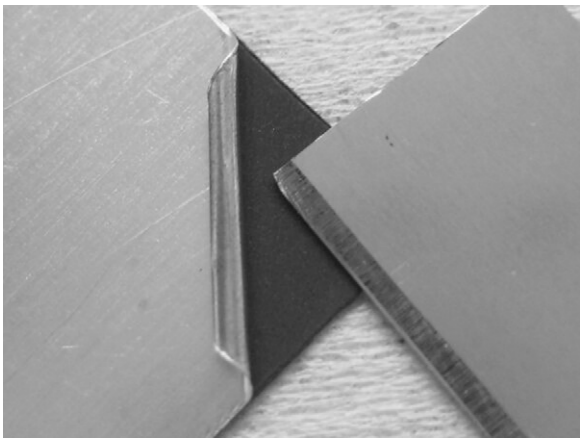

Fig. 3. Image showing procedure to remove aluminum current collector (curled top layer) from active-material film (bottom black layer) using a razor blade.

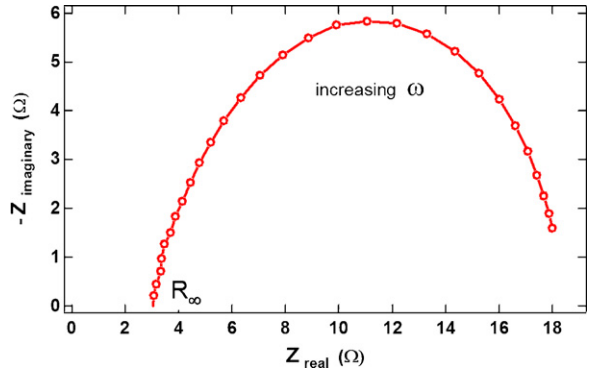

Fig. 4. Nyquist plot obtained from AC impedance experiment for separator cell shown in Fig. 1. The intercept with the real axis at high frequency (R_∞) is used to find the effective ionic conductivity in the separator region.

3.2.1. Polarization-interrupt experiment

The assembled cells (separator and active-material film cells) were tested using a battery tester (Maccor 4300, Maccor Inc.). Several conditioning cycles were performed on a cell to form a stable SEI (solid electrolyte interface) on the lithium electrodes. Each cycle consisted of passing a constant current (0.5 mA cm^{-2}) for 10 min, followed by a 3-min rest period, then passing current in the reverse direction under the same conditions. After the conditioning cycles, a constant current was applied for 2 min to set up a concentration gradient in the cell. Then, the concentration gradient was allowed to relax by interrupting the current until the cell potential approached zero. Then the current direction was reversed for 2 min followed by interruption of the current until cell potential approached zero. These steps were repeated for different current densities. The relaxation of the concentration gradient was observed in terms of a cell-potential decay with the time (Figs. 6 and 8). As discussed in more detail below, the model-experiment comparison (discussed in Section 5) of this cell-potential decay behavior was used to obtain quantitative information about the tortuosities of the porous structures.

3.2.2. AC impedance experiment

After the polarization-interrupt experiment, a current-controlled AC impedance test was performed using a frequency response analyzer (Gamry Instruments) on the separator cells to measure the total resistance between the two electrodes, R_∞. The frequency of the AC signal was varied from 100 Hz to 100 kHz at an amplitude of 0.025 mA cm^{-2}. R_∞ was taken from the intercept with the real axis at high frequency. Fig. 4 shows a representative Nyquist plot obtained from the AC impedance experiment for one of the cells. R_∞ is then used in conjunction with a model (see below) to obtain tortuosity for the separator.

4. Model development

In order to interpret each type of experiment and obtain a tortuosity value, the following models were used.

4.1. Polarization-interrupt experiment

The equations describing transport, kinetic, and thermodynamic processes in porous electrodes have been outlined previously [24–26]. In this work, during the polarization of a cell, lithium ions are generated at the anode surface, diffuse and migrate through the porous regions (separators and active-material film), and are deposited on the cathode. In order to model this system, the governing equations for the processes in the porous regions were implemented and solved using a finite element package (COMSOL Multiphysics 3.4) as described previously by Stephenson et al. [18]. However, because the cell geometry was not the same as that modeled by Stephenson et al., modifications to model geometry and the governing equations were made.

The separator and active-material film regions were modeled with a 1D restricted-diffusion geometry. The lithium metal anode and cathode (see Fig. 2) appear as boundary conditions in the model ($x = 0,\ L$). A brief summary of the governing equations and boundary conditions used in the model follows.

4.1.1. Charge transfer through the liquid phase

For the electrolyte phase, the governing equation for the porous regions is

$$\frac{\partial i}{\partial x} = 0, \tag{6}$$

where i is the superficial current density in the liquid phase and x is the position in the direction normal to the electrode surfaces.

We assume a binary electrolyte, no convection, and concentrated solutions with a constant cation transference number t_+^0. Given this, the current in the electrolyte can be expressed in a particular porous region by

$$i = -\kappa_{\text{eff}}\frac{\partial \phi}{\partial x} + \frac{2\kappa_{\text{eff}}RT}{F}\left(1 - t_+^0\right)\left(1 + \frac{d\ln f_\pm}{d\ln c}\right)\frac{\partial \ln c}{\partial x}, \tag{7}$$

where ϕ is the electric potential, R is the ideal gas constant, T is the temperature, F is the Faraday's constant, and c is the electrolyte concentration. The appropriate effective conductivity, κ_{eff}, for each porous layer was used. The activity coefficient correction, $1 + d\ln f_\pm/d\ln c$, in this work was taken to be one.

In a recent paper, Stewart and Newman [27] measured the activity coefficient correction for $LiPF_6$ in three different carbonate solvents, though not the mixed solvent used in this work. In each case the values increased with concentration, reaching a value around 2.5 in the case of 1 mol dm^{-3} $LiPF_6$ in 1:1 (w:w) EC/EMC. The polarization experiments in this work involved relatively small concentration variations about the average concentration of 1 mol dm^{-3}. Inclusion of a concentration-dependent correction factor in Eq. (7) therefore does not substantially influence the measured diffusive time constant of the relaxation period following polarization, and hence the calculated tortuosity results. All the potentials were taken relative to the lithium anode. The boundary condition at the anode surface ($x = 0$) is given by a Butler–Volmer expression (Eq. (6) in Ref. [18]). The exchange current density for the lithium metal electrodes was obtained by the AC-impedance method and was set to $i_0 = 0.41$ mA cm^{-2} at $c = 1$ mol dm^{-3}. The

boundary condition at the cathode side ($x = L$) is $i = I$, where I is the fixed current density being passed through the cell. The liquid-phase potential and superficial current are continuous at the porous-layer interfaces. A Butler–Volmer expression at the cathode electrode surface provides for the potential of the cathode relative to the anode. In effect the model sums the two kinetic overpotentials and the ohmic drop and concentration overpotential of each layer to obtain the cell potential.

4.1.2. Diffusion in the liquid phase

The continuity equation for mass transport is

$$\epsilon \frac{\partial c}{\partial t} = -\frac{\partial N}{\partial x}, \tag{8}$$

where N is the superficial molar flux of cations through the porous region and is calculated by

$$N = -D_{\text{eff}} \frac{\partial c}{\partial x} + \frac{i t_+^0}{F}, \tag{9}$$

where t_+^0 is the cationic transference number. The appropriate effective diffusivity, D_{eff}, for each porous layer was used. The boundary conditions at the electrodes ($x = 0, L$) are $N = I/F$. Also, electrolyte concentration and superficial molar flux are continuous at the porous-layer interfaces.

4.1.3. The intrinsic transport properties of the electrolyte

The intrinsic transport properties (D, κ, and t_+^0) used in this model are obtained directly or estimated from the literature. Recently, Stewart and Newman [23] measured the salt diffusion coefficient for $LiPF_6$ in 1:1 (w:w) EC/DEC by the method of restricted diffusion with concentration measured by ultraviolet/visible absorption. Their fit of the results is

$$D = 2.582 \times 10^{-5} \exp(-2.856c), \tag{10}$$

where D is in units $\text{cm}^2\,\text{s}^{-1}$ and c is in units $\text{mol}\,\text{dm}^{-3}$.

For conductivity of the electrolyte, we used a concentration-dependent shape function [18], scaled by an experimental value of the conductivity at a single concentration, namely $\kappa_{\text{ref}} = 7.8\,\text{mS}\,\text{cm}^{-1}$ at $c_{\text{ref}} = 1\,\text{mol}\,\text{dm}^{-3}$ for $LiPF_6$ in EC:DEC [28]. The resulting electrolyte conductivity used in this model is

$$\kappa = \kappa_{\text{ref}} \left(\frac{1.262(c/c_{\text{ref}})}{1 + 0.2(c/c_{\text{ref}})^2 + 0.08(c/c_{\text{ref}})^4} + 0.014 \right). \tag{11}$$

Note that the small non-zero value of κ at zero concentration was used in the model to ensure numeric stability generally, though in this particular work modeled concentrations never approached zero.

As for cationic transference number, we used a fixed value, $t_+^0 = 0.36$, in accordance with the earlier work employing this electrolyte [18].

4.2. AC impedance experiment

At high frequencies the concentration in an AC impedance experiment is effectively constant, which effects a significant simplification in the model. In addition, one can neglect the charge-transfer impedance at the electrode surfaces due to the low impedance of double-layer capacitance. This means that R_∞ can be directly related to electrolyte conductivity:

$$R_\infty = \frac{1}{A} \sum_j \frac{L_j}{\kappa_{j,\text{eff}}}, \tag{12}$$

where L_j and $\kappa_{j,\text{eff}}$ are the thickness and effective conductivity of layer j. The summation is over all porous layers between the two electrodes. A is the area of the electrodes normal to the current flow.

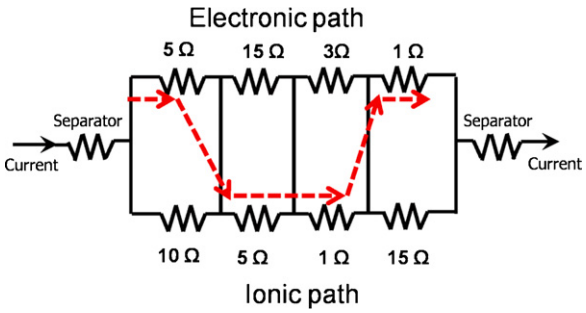

Fig. 5. Illustration of possible current paths in a cathode film. The current flows mostly through the least-resistance path (arrows), making unreliable the measurement of κ_{eff} without detailed knowledge of the local behavior of electronic and ionic paths.

Eq. (1) is used to calculate the tortuosity of the separator layers from the calculated/measured $\kappa_{j,\text{eff}}$ values and the intrinsic ionic conductivity.

The above formula does not work well for electronically conductive cathode films as used in our experiments. In the limit of high frequency and large interfacial area, the resistance for current flow between ionic and electronic pathways in the cathode becomes negligible. Thus, the alternating current is carried by both pathways, ionic and electronic, as illustrated in Fig. 5. The figure shows a resistive circuit representing the cathode film between two separator layers. The current will follow the least-resistance path, which may involve multiple hops between the ionic and electronic modes of transport. Therefore, determination of κ_{eff} is not straightforward.

As a further example, consider the continuum result for the same one-dimensional geometry of Fig. 5:

$$R_\infty = R_{\text{sep}} + R_{\text{surf}} + \frac{L}{(\kappa + \sigma)_{\text{avg}} A}, \tag{13}$$

$$\frac{1}{\sigma_{\text{avg}}} = \int_0^L \frac{1}{\sigma(x)}\,\text{d}x, \tag{14}$$

$$\frac{1}{\kappa_{\text{avg}}} = \int_0^L \frac{1}{\kappa(x)}\,dx, \tag{15}$$

where σ is the electronic conductivity and R_{surf} is an interfacial resistance, which will be explained later in this work (Eq. (17)). Functions $\kappa(x)$ and $\sigma(x)$ are the local variations in ionic and electronic conductivities respectively, The subscript 'avg' is used to indicate respective average quantities. What we seek is κ_{avg}, which is κ_{eff}, in order to compute the tortuosity. What the high-frequency AC impedance experiment provides by Eq. (13) is $(\kappa + \sigma)_{\text{avg}}$. It is also possible to perform dry conductivity measurements on the cathode film to obtain σ_{avg}. However, if local variations in ionic and electronic conductivities are negatively correlated (as we expect from physical arguments) then $(\kappa + \sigma)_{\text{avg}} > (\kappa_{\text{avg}} + \sigma_{\text{avg}})$. In summary, because the local correlations of conductivities $\kappa(x)$ and $\sigma(x)$ are unknown, we make no attempt in this work to extract κ_{avg} and hence τ from R_∞ values. We nevertheless believe there is important information that can be obtained from such experiments when combined with appropriate modeling, but such is beyond the scope of the present work.

The problem just outlined is not present for separator-only experiments where $\sigma \approx 0$. Therefore, we used AC-impedance to find the tortuosity of the separator layers and to serve as a validation for the polarization interrupt experiment on the same system. The polarization interrupt experiment is then used solely to determine the tortuosity in the active-material films.

5. Results and discussion

5.1. Tortuosity in the separator

5.1.1. AC measurements

Because the conductivity measurements were done at high AC-signal frequency, there is negligible concentration variation in the cell: $c = c_{ref}$. Therefore, we take $\kappa = \kappa_{ref}$. From this and the effective conductivity (κ_{eff}), the apparent tortuosity (τ_{app}) for the separator was calculated using Eq. (1). This experiment was repeated using different numbers of separators and the apparent tortuosity of the separators was calculated in each instance. Then, the results for the tortuosity for different numbers of separators were compared with those obtained from the polarization-interrupt (Fig. 7).

5.1.2. Restricted-diffusion measurements

Fig. 6 shows results on a semi-log plot from a representative experiment containing three separator layers, compared to the corresponding model results. The cell was polarized for 2 min at a constant current density (1.25 mA cm^{-2}) and then the current was interrupted for 10 min, during which the cell potential approached zero. As discussed previously, the procedure was repeated for different current densities and polarities. The tortuosity in the model was varied to best reproduce the experimental relaxation time constant (slope on the semi-log plot). The best tortuosity was taken to be the one that minimized the sum of squared error during the first 2 min of the relaxation period. The same fitting procedure was repeated for different current densities to validate and average the results. The model curves showed good agreement with corresponding experimental curves, as illustrated in Fig. 6.

Fig. 7 shows the apparent tortuosity (τ_{app}) as a function of number of the separators (N), as obtained from AC-impedance and polarization-interrupt experiments. One can think of the vertical axis ($\tau_{app}N$) as a dimensionless total resistance between the electrodes. The first thing to note is the satisfactory agreement between the AC-impedance and restricted-diffusion experiments. Also shown in the figure is a linear fit for the combined experimental data set. The slope of the fit represents the actual tortuosity of the separator layers, calculated here for Celgard 2400 to be $\tau = 3.15$. However, the apparent tortuosity measured for one separator is $\tau_{app} = 6.12$ which is in good agreement with $\tau_{app} = 5.98$ obtained by Patel et al. [12]. It is perhaps surprising that τ is so large for this material given that the pores are sometimes represented as being straight and parallel. Instead, $\tau > 1$ and the effective transport properties are much reduced relative to that ideal.

5.1.3. Interfacial resistance

Interestingly, the intercept of the fit in Fig. 7 does not go to zero. This suggests that there was an additional resistance in the system, not associated with the separators themselves, but instead associated with the surfaces of the lithium electrodes. This interfacial resistance could be due to the solid electrolyte interphase (SEI) or some kind of interfacial spreading resistance or both. For instance, active redox sites on the electrode surface are not necessarily aligned with the separator pores and spreading resistance could be incurred. Also of note is that this interfacial resistance has two aspects: ohmic resistance and diffusional resistance, as given by the fact that the AC-impedance and polarization-interrupt results have essentially the same intercept in Fig. 7. Additional work is needed to determine any electrolyte-composition dependence of this resistance.

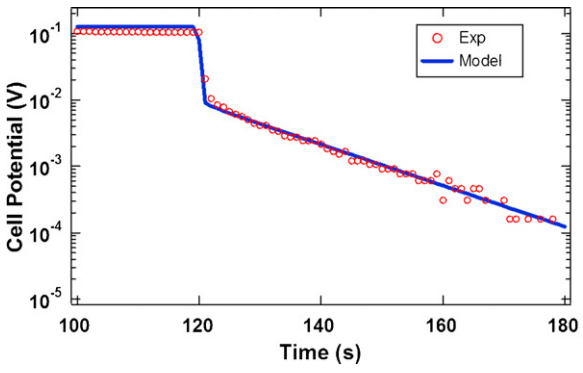

Fig. 6. Model-experiment comparison for galvanostatic polarization ($t < 120$ s), followed by interrupt and relaxation ($t > 120$ s) in a cell containing three separators.

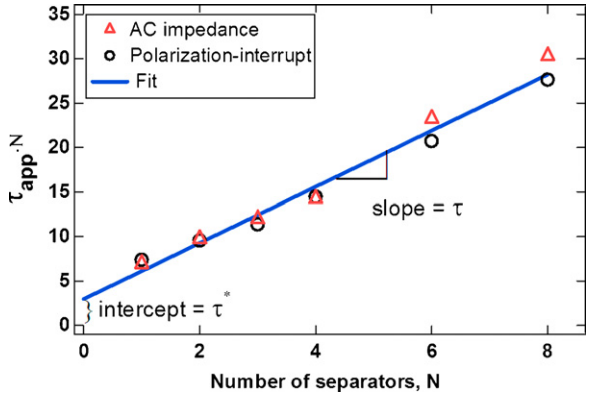

Fig. 7. The variation of the apparent tortuosity τ_{app} with the number of separators. The data suggest good agreement between the AC-impedance and polarization-interrupt experiments. The slope of the linear fit corresponds to the true tortuosity, while the non-zero intercept suggests a surface resistance at the lithium electrodes.

There are multiple ways one could take into account this additional interfacial resistance. It is not accurate, however, to model it solely as an electrical resistance, as this would neglect the concentration polarization that happens as well. In the present model we included the interfacial resistance by taking it to be a thin surface layer, essentially a porous separator, placed next to each electrode. To do this we assumed a thickness of the layer, $L_{surf} = 2.5$ μm, and a porosity, $\epsilon_{surf} = \epsilon_{sep} = 0.37$. The intercept τ^* of Fig. 7 and the thickness of the normal separator layer L_{sep} are then used to calculate an effective tortuosity of the surface layer:

$$\tau_{surf} = \tau^* \frac{L_{sep}\epsilon_{surf}}{2L_{surf}\epsilon_{sep}} = 14.8. \quad (16)$$

The particular values used for L_{surf} and ϵ_{surf} are not important as long as this additional surface layer has the appropriate overall resistance and occupies a negligible volume fraction of the cell, and numerical stability can be maintained in the model. Because we model the interfacial resistance as a distinct layer next to each electrode, we use the true tortuosity of the separators (the slope in Fig. 7) rather than the apparent tortuosity to model the polarization-relaxation experiments of the cells containing cathode films. Finally we note that in the case of the AC impedance experiment represented in Eq. (13), the total high-frequency resistance associated with the two electrode surface layers is

$$R_{surf}A = \frac{2L_{surf}\tau_{surf}}{\kappa\epsilon_{surf}} = 2.56\,\Omega\,\text{cm}^2. \quad (17)$$

5.2. Tortuosity in the active-material films

To better understand the effect of morphology and porosity on the tortuosity of cathode-material films, the polarization-interrupt experiment was performed on cells of different compositions and porosities. The main focus in this paper is on the relationship between porosity and tortuosity for $LiFePO_4$ cathodes, with a goal

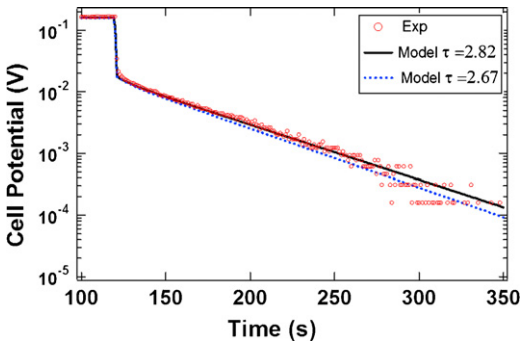

Fig. 8. Model-experiment comparison for polarization and relaxation in the $LiFePO_4$ film. Two model curves are shown: the first is considered the best fit of the relaxation data. The second is shown to illustrate the sensitivity of the model result to tortuosity by using a value that differs from the best fit by 5%.

to develop an empirical correlation (like the Bruggeman relation) between these two variables. However, some additional cells containing $LiCoO_2$ active material were tested as well.

5.2.1. Restricted-diffusion measurements

As with the separator-only cells, the detailed model is used to regress the tortuosity. In this case the tortuosity of the separator layers (and electrode surface layers) are fixed and the tortuosity of the cathode film is varied to best fit the time constant of the relaxation curves.

Fig. 8 shows a representative semi-log plot of model-experiment comparison of the polarization-relaxation experiment for a $LiFePO_4$ film (115 μm thick, $\epsilon = 0.45$). The cell was polarized for 2 min with a constant current density (1.25 mA cm^{-2}) and then the curre nt was interrupted, causing the cell potential to approach zero. Shown in the figure are two model results. The first curve is the best fit of τ from the relaxation time constant (slope in the plot). In the second model curve τ was purposely offset from the optimum by 5% in order to illustrate the sensitivity of the model to changes in τ.

A statistical analysis was performed for a single cell to determine a characteristic uncertainty for the obtained tortuosities. The model was independently fit to the relaxation results for five different polarization current densities. These independent samples yielded a standard error of 1.1% in tortuosity at the 90% confidence level. In addition to this measurement uncertainty, another source of error is the cell-to-cell variation due to imperfect fabrication and natural material differences, as apparent in Fig. 9.

5.2.2. Tortuosity-porosity correlation

Accurate cell modeling for prediction and optimization requires accurate transport properties. To aid in this type of modeling we present Fig. 9, which summarizes the effect of porosity on the tortuosity of the tested cathode films, with the focus being on $LiFePO_4$ films. A power function is fit to the data and shown in the figure. The root-mean-square fractional deviation of experimental points from the fit is 2.7%. The maximum absolute fractional deviation for any point is 4.7%. This means that the experimental points are well described by the correlation

$$\tau = 1.8\epsilon^{-0.53}. \quad (18)$$

This means $\alpha = 1.53$ in Eq. (4), which is nearly same as that recommended by Bruggeman [14]. However, the tortuosity obtained in this work is nearly two times ($\gamma = 1.8$) higher than that predicted by the Bruggeman relation. This suggests that the effective transport properties can be well predicted by a scaled Bruggeman relationship. The scaling parameter γ can be adjusted for different constituents and particle morphologies of the active-material film. Nevertheless, in Fig. 9 the few results for $LiCoO_2$-material films (indicated by triangles) and carbon-fiber-containing $LiFePO_4$-material films (indicated by squares) show good agreement with the baseline $LiFePO_4$ results. In these cases either the active-material differs with respect to particle shapes and sizes, or the carbon aspect ratio differs, but the relative mass fractions of active material, carbon additive, and binder are the same.

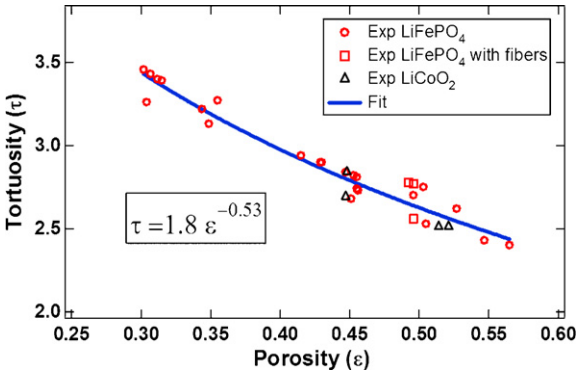

Fig. 9. The effect of porosity on the tortuosity of cathode films. The tortuosity is well correlated by a power-law equation (inset).

Some researchers have used the Bruggeman exponent as an adjustable parameter in full battery simulations and arrived at a relatively large value [10,13]. However, it is possible that the large exponent compensates for assuming a unity scaling factor or other possible model deficiencies. Prior work by our group [18] used the normal Bruggeman exponent ($\alpha = 1.5$); however, the scaling factor was much larger ($\gamma = 21$) than obtained here. This was needed to obtain apparent concentration-polarization effects observed for a thick cell under high-rate discharges. However, that work did not use a concentration-dependent liquid-phase diffusivity. Using the diffusion correlation by Stewart and Newman [23], in which D can take quite small values at large concentrations, better enables the model to reproduce high-rate discharges for thick cathodes without resorting to such a large scaling factor. In addition, the earlier work did not entail a direct measure of liquid-phase transport. We therefore believe the present work to be a more reliable indication of the tortuosity in typical porous cathodes for lithium-ion batteries. The Bruggeman relationship has been shown to be accurate for a conductive phase mixed with monodisperse insulated spherical particles [12,14,16,17]. TEM images of $LiFePO_4$ (Fig. 10) suggest a non-monodisperse and non-spherical particle morphology for the system. The addition of carbon additives (carbon black, graphite, and carbon fibers) in such cells further distorts the pore structure from the Bruggeman ideal. It appears that the Bruggeman relation is a limiting case for particulate systems; realistic (non-monodisperse and non-spherical) systems will have greater tortuosity than given by Bruggeman.

5.2.3. Model validation with different thicknesses

To optimize batteries for HEV and PHEV, it is also desirable to know the effect of different resistances with the thickness of the electrode [29]. Our present work helps to predict the liquid phase resistance with different thicknesses of the electrode. By incorporating the tortuosity in the separator, interfacial resistance on lithium electrodes, and tortuosity of the active-material film, the model can be used to predict the diffusive time constant for different active-material film thickness. The results shown in Fig. 9 at $\epsilon = 0.45$ are for cathode films around 100 μm thick. Fig. 11 shows results for a thicker (140 μm, $\epsilon = 0.45$) $LiFePO_4$ film, with the model operated in predictive mode. The agreement between model prediction and experiment is good in terms of the correct relaxation slope on the semi-log plot. This supports the validity of our tortuosity-porosity correlation (Eq. (18)) for different thicknesses.

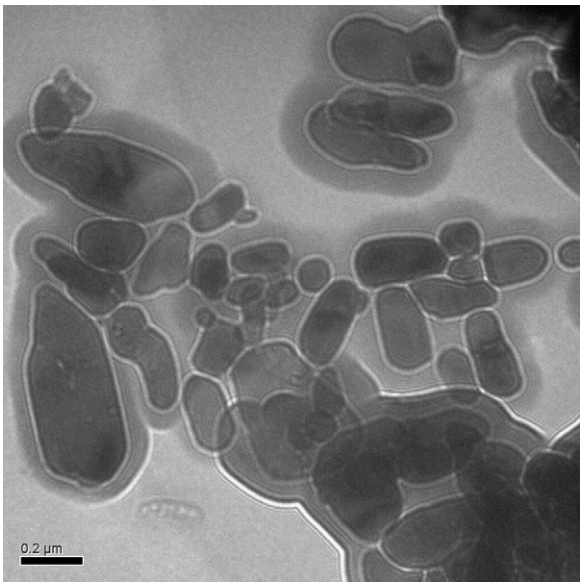

Fig. 10. TEM image of $LiFePO_4$ particles suggesting a non-monodisperse and non-spherical particle distribution.

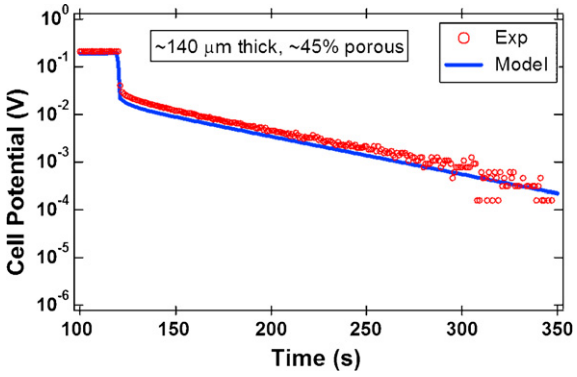

Fig. 11. Transport model validation from a polarization-interrupt experiment for a thicker $LiFePO_4$ cathode film (140 μm) at 45% porosity, where the effective transport properties in the model are parametrized from experiments on thinner (≈100 μm) cells. The good agreement between the model and experiment in terms of relaxation decay rate suggests the tortuosity correlation given in the text is accurate for different thicknesses.

6. Conclusion

In order to have a model that can accurately predict cell performance under varying fabrication parameters and operating conditions, it is imperative to have accurate transport properties in the model. In this study, experimental and modeling methods to determine the tortuosity in the separator and the active-material film were developed. The tortuosity is a geometric parameter independent of the particular electrolyte used; its value is needed to predict effective conductivity and diffusivity in a porous material.

AC impedance and a polarization-interrupt (or restricted diffusion) experiment with a special cell geometry were used to measure directly the tortuosity in the separator and the active-material films. Nevertheless, and particularly in the case of the active-material films, interpretation of the experiments requires a detailed mathematical model. The tortuosities for the separator obtained from the two types of experiment were consistent with each other. This suggests that a restricted-diffusion-type experiment can be used reliably to determine the tortuosity of a porous structure. Therefore, the tortuosity of the active-material films was extracted from the model-experiment comparison of the polarization-interrupt experiments.

Our experiments for the separator uncovered an interfacial resistance associated with the surface of the lithium electrodes that prior researchers may have inadvertently included in the resistance assigned to the separator, hence our use of the term "apparent tortuosity." The apparent tortuosity we obtained for one separator layer was found to be in good agreement with values reported by others. A separate accounting for the interfacial layer leads to the true tortuosity of the separator; we expect this value to be more appropriate in cell modeling.

Also interesting is that our experiments suggest this interfacial layer restricts salt diffusion with the same tortuosity as it does ionic current, at least for the particular electrolyte used here. The surface resistance can be modeled as an additional porous layer adjacent to each lithium metal electrode. Our prior experience suggests concentration depletion can occur in lithium batteries cycled at high rates ($\approx 5\,C$) and thus have a significant effect on cell voltage. Therefore it is important to correctly account for diffusive resistances in separators and surface films as well as in the porous electrodes. In addition, one must correctly account for the concentration dependence of the liquid diffusivity.

A correlation between tortuosity and porosity of active-material films was obtained. The oft-used Bruggeman exponent ($\alpha = 1.5$) seems to predict the porosity dependence of tortuosity quite well. However, the tortuosities of the porous structures studied in this work, both the separator and active-material films, are approximately two times larger than those predicted by the Bruggeman relation. In particular for the separator this confirms that the transport paths are not straight parallel channels.

The experimental techniques and models developed in this work can be used to determine the transport resistances for cathode films with different porosities and thicknesses. This can help in optimizing batteries for different applications. Once the factors that affect the different transport resistances are quantified, fabrication strategies can be developed to mitigate the dominant resistances. For instance, lower porosity is desired for lower electronic resistance [19]. On the other hand, higher porosity or liquid-volume fraction is desired for lower liquid-phase resistance. Therefore, there is a trade-off between electronic and liquid-phase resistance with porosity [29]. Once the electronic resistance is known, our model and experimental methods can be used to predict such an optimum point for cell fabrication for a particular application.

Acknowledgements

This work was supported by the BATT program of the U.S. Department of Energy under Contract No. DE-AC02-05CH11231 and Naval Research Laboratory under grant N00173-08-2-C012. We acknowledge Dr. Richard R. Vanfleet (Dept. of Physics and Astronomy, Brigham Young University) for assisting in TEM image analysis of $LiFePO_4$. Brigham Young University assisted in meeting the publication costs of this article.

References

[1] R. Pollard, J. Newman, J. Electrochem. Soc. 128 (1981) 491.
[2] Y.Q. Lei, et al., J. Alloys Compd. 231 (1995) 611.
[3] T.F. Fuller, M. Doyle, J. Newman, J. Electrochem. Soc. 141 (1) (1994) 1.
[4] G.G. Botte, V.R. Subramanian, R.E. White, Electrochim. Acta 45 (2000) 2595.
[5] R. Darling, J. Newman, J. Electrochem. Soc. 145 (1998) 990.
[6] C. Wang, U.S. Kasavajjula, P.E. Arce, J. Phys. Chem. C 111 (2007) 16656.
[7] P.P. Prosini, J. Electrochem. Soc. 152 (10) (2005) A1925.
[8] V. Srinivasan, J. Newman, J. Electrochem. Soc. 151 (2004) 1517.
[9] P. Arora, R.E. White, M. Doyle, J. Electrochem. Soc. 145 (1998) 3647.
[10] M. Doyle, J. Newman, A.S. Gozdz, N. Schmutz, J.-M. Tarascaon, J. Electrochem. Soc. 143 (1996) 1890.
[11] K. Abraham, Electrochim. Acta 38 (1993) 1233.
[12] K.K. Patel, J.M. Paulsen, J. Desilvestro, J. Power Sources 122 (1993) 1233.

[13] D. Fan, R.E. White, J. Electrochem. Soc. 138 (1991) 17.
[14] D.A.G. Bruggeman, Ann. Phys. 24 (1935) 636.
[15] R.E. Meredith, C.W. Tobias, Adv. Electrochem. Electrochem. Eng. 2 (1962) 15.
[16] R.M.D.L. Rue, C.W. Tobias, J. Electrochem. Soc. 106 (1959) 827.
[17] R.B. MacMullin, G.A. Muccini, AIChE J. 2 (1956) 393.
[18] D.E. Stephenson, E.M. Hartman, J.N. Harb, D.R. Wheeler, J. Electrochem. Soc. 154 (12) (2007) 1146.
[19] C.-W. Wang, Y.-B. Yi, A.M. Sastry, J. Shim, K.A. Striebel, J. Electrochem. Soc. 151 (2004) 1489.
[20] D. Djian, F. Alloin, S. Martinet, H. Lingnier, J.Y. Sanchez, J. Power Sources 172 (2007) 416.
[21] M. Pavlin, T. Slivnik, D. Miklavčič, IEEE Trans. Biomed. Eng. 49 (1) (2002) 80.
[22] J. Newman, T.W. Chapman, AIChE J. 19, 1973 (343).
[23] S.G. Stewart, J. Newman, J. Electrochem. Soc. 155 (2008) F13.
[24] P. Ramadass, B. Haran, R. White, B.N. Popov, J. Power Sources 123 (2003) 230.
[25] J. Newman, K.E. Thomas-Alyea, Electrochemical Systems, John Wiley and Sons, 2004.
[26] K.E. Thomas, R.M. Darling, J. Newman, Advances in Lithium-Ion Batteries, Kluwer Academic/Plenum Publishers, 2002 (Chapter 12).
[27] S. Stewart, J. Newman, J. Electrochem. Soc. 155 (2008) 458.
[28] Battery Materials, Tech. Rep., EM Industries, 7 Skyline Drive, Hawthorne, NY 10532, 1998.
[29] I.V. Thorat, V. Mathur, J.N. Harb, D.R. Wheeler, J. Power Sources 162 (2006) 673.